Magnetic correlations and the influence of atomic disorder in frustrated isosceles triangular lattice antiferromagnet $CuMnO_2$

Noriki Terada, Yoshinori Tsuchiya, and Hideaki Kitazawa
National Institute for Materials Science, Sengen 1-2-1, Tsukuba, Ibaraki 305-0047, Japan

Toyotaka Osakabe, Naoto Metoki, and Naoki Igawa
Japan Atomic Research Agency, Tokai, Ibaraki 319-1195, Japan

Kenji Ohoyama
Institute for Materials Research, Tohoku University, Katahira, Sendai 980-8577, Japan
(Received 25 May 2011; revised manuscript received 31 July 2011; published 26 August 2011)

We have studied the magnetic correlations of the isosceles triangular lattice antiferromagnet $Cu_{1+x}Mn_{1-x}O_2$ with $x = 0.00$ and 0.04, using the magnetic susceptibility, specific heat, elastic, and inelastic neutron-scattering experiments. Above T_N, the magnetic correlations in both samples are characterized by a two-dimensional (2D) short-range correlation, as indicated by the broad peak in the susceptibility and the asymmetric diffuse scattering observed in neutron diffraction experiments. Below T_N, the magnetic structures, with the propagation vectors $\boldsymbol{Q} = (\frac{\bar{1}}{2}\frac{1}{2}\frac{1}{2})$ in $x = 0.00$ and $\boldsymbol{Q} = (\frac{\bar{1}}{2}\frac{1}{2}0)$ in $x = 0.04$, have been identified to be collinear magnetic structures with the magnetic moments almost parallel to the d_{z^2} orbitals. Although the atomic disorder does not affect the direction and length of the magnetic moments in $CuMnO_2$, the stacking sequence along the c direction is changed from antiferromagnetic to ferromagnetic. Considering the interlayer exchange interactions between isosceles triangular lattice layers, we find that the second-nearest-neighbor interlayer interaction plays an important role for the magnetic stacking along the c axis. The magnetic excitation below T_N is characterized by collective spin-wave excitation with an energy gap of 6 meV from the three-dimensional long-range magnetic order and by spin-liquid-like 2D excitation, as indicated by $C(T) \propto T^2$ in $CuMnO_2$.

DOI: 10.1103/PhysRevB.84.064432 PACS number(s): 75.10.Kt, 75.25.−j, 75.30.Ds, 75.50.Ee

I. INTRODUCTION

In recent years, there has been renewed interest in geometrically frustrated magnetic systems. In such systems, spin ordering is suppressed by competing exchange interactions well below the conventional ordering scale set by the Weiss temperature. Consequently, they are expected to possess unconventional magnetic states, such as spin-liquid[1] and spin-nematic states.[2] ABO_2-type materials, which have two-dimensional (2D) layered structures consisting of triangular lattices made up of magnetic B-site trivalent cations, have been studied as typical frustrated triangular-lattice spin systems.[3] In particular, $CuFeO_2$ and $CuCrO_2$ have been extensively studied in terms of magnetoelastic coupling and magnetoelectric multiferroics, which are considered to be associated with spin frustration.[4–7]

Crednerite $CuMnO_2$ is an ABO_2-type triangular-lattice antiferromagnet. Unlike other ABO_2-type materials that have B-site cations of Fe^{3+} ($3d^5$: $t_{2g}^3e_g^2$) and Cr^{3+} ($3d^3$: t_{2g}^3), the crystal structure of $CuMnO_2$ does not consist of perfect triangular lattices, rather it consists of isosceles-triangular lattices due to Jahn-Teller distortion of Mn^{3+} ($3d^4$: $t_{2g}^3e_g^1$) with an orbital degree of freedom. The crystal structure of $CuMnO_2$ is illustrated in Fig. 1. The crystal structure of $CuMnO_2$ belongs to the monoclinic space group $C2/m$ at room temperature and it has lattice constants of $a = 5.596$ Å, $b = 2.880$ Å, $c = 5.899$ Å, and $\beta = 104.02°$.[8] Doumerc *et al.* performed magnetic susceptibility measurements of $CuMnO_2$; the electronic configuration of Mn^{3+} was found to be the high spin state ($S = 2$) and a Weiss temperature Θ_{CW} is −407 K.[10] They also used Mössbauer spectroscopy to investigate ^{57}Fe-doped samples and found a 3D long-range magnetic ordering below $T_N = 64$ K.[10] In the intermediate temperature regions of $T_N < T < \Theta_{CW}$, the susceptibility shows broad peaks reflecting the low-dimensional character. So far, the microscopic magnetic correlations and the dimensionality have not been clarified.

The recent neutron diffraction studies have revealed the magnetic structure of $CuMnO_2$ and the crystal structure deformation associated with the magnetic ordering.[11,12] The magnetic structure below $T_N = 64$ K is the collinear one with the magnetic propagation vector $\boldsymbol{Q}_1 = (\frac{\bar{1}}{2}\frac{1}{2}\frac{1}{2})$. In addition to $\boldsymbol{Q}_1$, they observed the other group of the magnetic Bragg reflections which are assigned by $\boldsymbol{Q}_2 = (\frac{\bar{1}}{2}\frac{1}{2}0)$. While the intensity for $\boldsymbol{Q}_1$ is dominant, that for $\boldsymbol{Q}_2$ is speculated to be caused by a small amount of impurity of $Cu_{1+x}Mn_{1-x}O_2$.[11] Trari *et al.*[9] reported the magnetic susceptibility of $Cu_{1+x}Mn_{1-x}O_2$ with $0.0 \leqslant x \leqslant 0.20$, suggesting that the magnetic susceptibility is highly sensitive to the atomic disorders. However, the minor fraction for $\boldsymbol{Q}_2$ has not been investigated thus far. The structural phase transition also occurs below T_N from the monoclinic $C2/m$ to the triclinic $C\bar{1}$ in $CuMnO_2$.[11,12] The degeneracy in the exchange interaction paths between base sites and apex sites in isosceles triangular lattice, J_2, is lifted by the distortion.

In order to investigate the detailed magnetic correlation in $CuMnO_2$, and the atomic disorder effect, we have performed the magnetic susceptibility, specific heat, elastic, and inelastic neutron-scattering experiments on $Cu_{1+x}Mn_{1-x}O_2$ with $x = 0.00$ and 0.04.

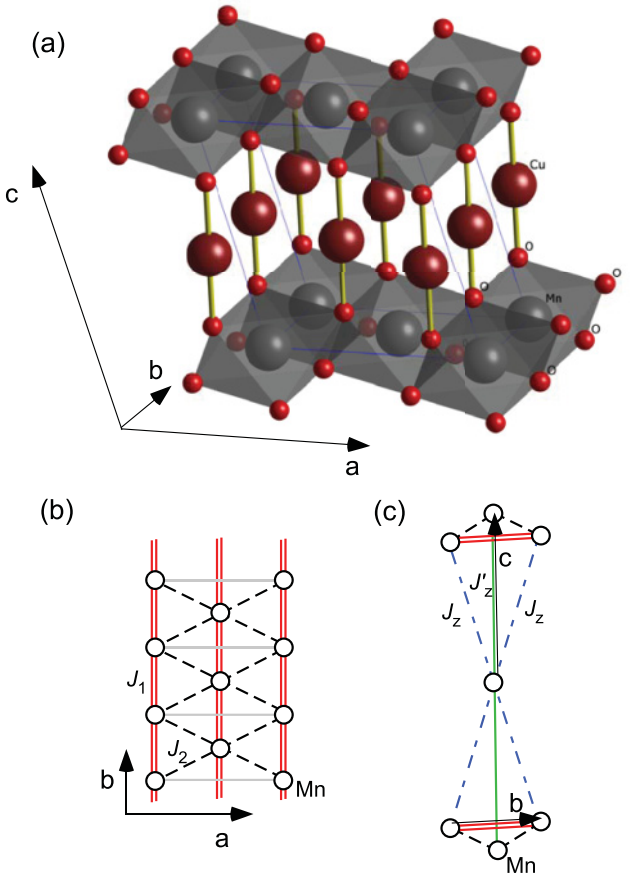

FIG. 1. (Color online) (a) Crystal structure of crednerite $CuMnO_2$ with the monoclinic unit cell. (b) Schematic picture of isosceles triangular lattice layer with the nearest-neighbor and the next-nearest-neighbor exchange interactions, J_1 and J_2. The interlayer exchange interactions are illustrated in (c).

II. EXPERIMENTAL DETAILS

Powder samples of $Cu_{1+x}Mn_{1-x}O_2$ were synthesized by a solid-state reaction. This reaction was performed for 24 h in vacuum-sealed quartz tubes. It is described by

$$(1+x)Cu_2O + (1-x)Mn_2O_3 \rightarrow 2Cu_{1+x}Mn_{1-x}O_2.$$

The starting oxides were accurately weighed and mixed in an alumina mortar with ethanol for about 1 h until dry. They were then pressed into pellets. According to Trari *et al.*, the reaction temperatures to synthesize a pure sample of $CuMnO_2$ and a sample with a slight excess of Cu, $Cu_{1+x}Mn_{1-x}O_2$ with $x = 0.05$, are 950 and 970 °C, respectively. For both samples, two grindings and firings were required to obtain a single phase. X-ray powder diffraction measurements confirmed that the obtained samples consisted of a single phase. The Cu excess, x, was measured by inductively coupled plasma-optical emission spectrometry and found to be $x = 0.00$ and $x = 0.04$ in the two samples. We used a magnetic-property measurement system (Quantum Design) for magnetic susceptibility measurements and a physical property measurement system (Quantum Design) for specific heat measurements.

Elastic neutron-scattering experiments were conducted using the HERMES, HRPD, and MUSASI diffractometers installed at JRR3 in Tokai, Japan, with incident wavelengths, λ, of 1.8204, 1.8244, and 2.55 Å, respectively. About 1 g of sample was used in each measurement. Inelastic neutron-scattering experiments were performed on 8 g $CuMnO_2$ powder using a triple-axis spectrometer TAS-2 at JRR3. The TAS-2 was operated in constant $E_f = 14.7$ meV mode with horizontal collimations 40′-80′-80′-open. A pyrolytic graphite filter installed behind the sample was used to remove higher-order contamination of scattered neutrons. In all the neutron diffraction measurements, the samples were cooled using a closed-cycle He refrigerator.

III. RESULTS AND DISCUSSIONS

A. Magnetic orderings in $Cu_{1+x}Mn_{1-x}O_2$

1. Magnetic susceptibility measurements

Figure 2 shows the temperature dependences of the magnetic susceptibility, $\chi(T)$, for $CuMnO_2$ and $Cu_{1.04}Mn_{0.96}O_2$. In both samples, $\chi(T)$ shows a broad peak with a maximum at temperatures of 160 K for $CuMnO_2$ and 130 K for $Cu_{1.04}Mn_{0.96}O_2$. This $\chi(T)$ behavior is generally observed in low-dimensional Heisenberg spin systems, such as the one-dimensional system $CsMnCl_3 \cdot 2H_2O$ (Ref. 13) and the 2D system K_2NiF_4.[14] With further decreasing temperature, $\chi(T)$ decreases rapidly at 64 and 52 K in $CuMnO_2$ and $Cu_{1.04}Mn_{0.96}O_2$, respectively. This anomaly is considered to indicate stabilization of a 3D long-range order. The magnetization $CuMnO_2$ increased steeply below 45 K. These results are consistent with previous magnetization measurements.[10] The increase in the magnetization has been suggested to be caused by a small amount of the impurity Mn_3O_4, which exhibits a ferromagnetic phase transition at ∼45 K.[12] We did not observe any significant anomaly in the temperature dependence of the specific heat or neutron scattering. On the other hand, $\chi(T)$ of $Cu_{1.04}Mn_{0.96}O_2$ shows no enhancement corresponding to ferromagnetism. Since the enhancement below ∼30 K is much smaller than that observed in $CuMnO_2$, it is considered to be caused by a small amount of paramagnetic impurity.

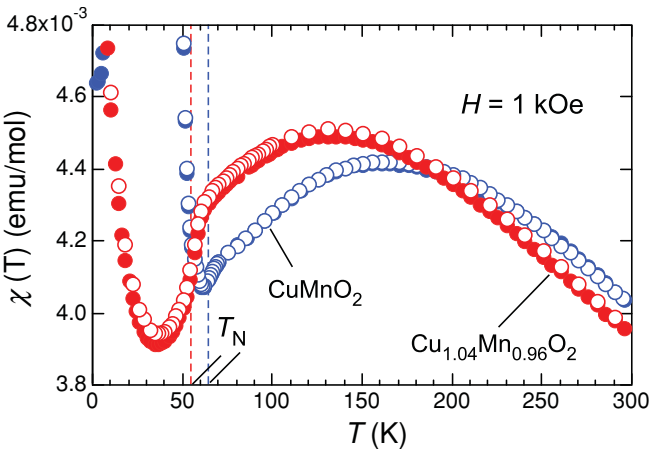

FIG. 2. (Color online) Magnetic susceptibilities of $CuMnO_2$ and $Cu_{1.04}Mn_{0.96}O_2$. Data were obtained under $H = 1$ kOe. Open and closed symbols denote field-cooling and zero-field-cooling data, respectively.

2. *Neutron diffraction experiments*

We performed neutron diffraction experiments on $CuMnO_2$ and $Cu_{1.04}Mn_{0.96}O_2$. A previous study has reported neutron diffraction data and analysis for $CuMnO_2$.[11,12] As shown in Fig. 3(a), we observed magnetic Bragg reflections, in addition to nuclear reflections, below T_N. Two magnetic wave vectors, which can explain the magnetic peaks, were observed: $\boldsymbol{Q}_1 = (\bar{\frac{1}{2}}\frac{1}{2}\frac{1}{2})$ and $\boldsymbol{Q}_2 = (\bar{\frac{1}{2}}\frac{1}{2}0)$. The intensity for $\boldsymbol{Q}_1$ is dominant, while the component for $\boldsymbol{Q}_2$ is relatively small, as the inset of Fig. 3(a) clearly shows. We used the FULLPROF program[15] to refine the magnetic structure for the main component with $\boldsymbol{Q}_1$. However, the secondary component with $\boldsymbol{Q}_2$ was so small that the refinement was unsuccessful. Figure 3(a) shows the fitting results for data obtained at 300 and 10 K and Table I lists the refined parameters. The magnetic structure of $\boldsymbol{Q}_1$ in $CuMnO_2$ was found to be collinear with the magnetic moments almost parallel to the d_{z^2} orbital, which is consistent with the results of previous studies.[11,12]

We observed the neutron diffraction profile of $Cu_{1.04}Mn_{0.96}O_2$ below T_N, as shown in Fig. 3(b). According

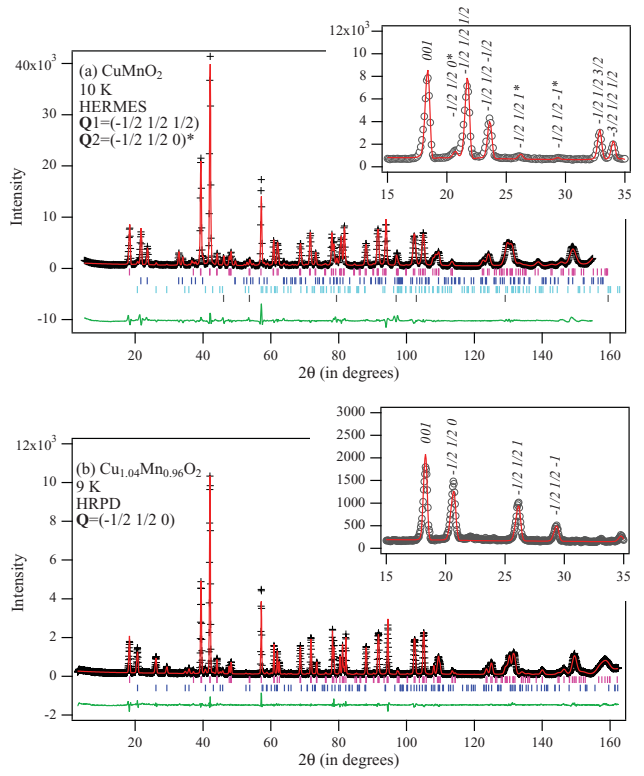

FIG. 3. (Color online) Neutron powder diffraction refinement pattern (a) at 10 K for $CuMnO_2$ and (b) at 9 K for $Cu_{1.04}Mn_{0.96}O_2$. The vertical bars at the bottom indicate the Bragg reflection positions. (a) Top, second, third, and bottom bars correspond to the crystal structure with $C\bar{1}$, the first magnetic phase with $\boldsymbol{Q}_1 = (\bar{\frac{1}{2}}\frac{1}{2}\frac{1}{2})$, the second magnetic phase with $\boldsymbol{Q}_2 = (\bar{\frac{1}{2}}\frac{1}{2}0)$, and aluminum contamination phase, respectively. (b) Upper and lower vertical bars correspond to crystal and magnetic phases, respectively. The lowest curve is the difference between the observed and calculated intensity. The inset shows enlarged patterns with peak assignment for 2θ between 15° and 35°. Asterisks after the indices denote the magnetic reflection for $\boldsymbol{Q}_2 = (\bar{\frac{1}{2}}\frac{1}{2}0)$.

TABLE I. Rietveld refinement results of the neutron powder diffraction data for $Cu_{1+x}Mn_{1-x}O_2$ with $x = 0.00$ and 0.04. Cu and Mn cations occupy sites $2d$ $(0\frac{1}{2}\frac{1}{2})$ and $2a$ (0 0 0), respectively.

x	0.00	0.00	0.04	0.04
Temperature	300 K	10 K	200 K	9 K
Instrument	HERMES	HERMES	MUSASI	HRPD
Space group	$C2/m$	$C\bar{1}$	$C2/m$	$C\bar{1}$
Cell parameters				
a (Å)	5.5934(1)	5.5723(1)	5.5842(3)	5.5536(1)
b (Å)	2.8824(1)	2.8780(1)	2.8927(2)	2.8804(1)
c (Å)	5.8895(1)	5.8902(1)	5.9132(3)	5.8939(1)
α (deg)	90	90.18(1)	90	90.12(1)
β (deg)	103.95(1)	103.94(1)	104.15(1)	104.14(1)
γ (deg)	90	89.84(1)	90	89.87(1)
Atomic positions				
O(4i) x	0.4065(3)	0.4065(3)	0.4065(6)	0.4059(2)
O(4i) y	0	−0.0001(2)	0	0.0003(4)
O(4i) z	0.1786(4)	0.1785(3)	0.1787(4)	0.1787(2)
R_{Bragg}(%)	4.33	3.13	4.92	2.35
R_F(%)	2.93	2.27	3.40	1.54
R_{wp}(%)	14.6	15.3	10.5	11.3
R_e(%)	7.32	3.48	5.12	7.52
Magnetic moment				
M_a (μ_B)		2.85(5)		2.83(3)
M_c (μ_B)		1.84(11)		1.53(6)
$R_{\text{Bragg magnetic}}$(%)		14.1		15.6

to the consideration for atomic disorder of $Cu_{1+x}Mn_{1-x}O_2$ in the previous paper,[9] the excess of Cu ions would hold on the deficient B sites as Cu^{2+}, and the same amount of Mn^{3+} could also change into Mn^{4+}. In this analysis, we assumed that A sites are fully occupied by Cu^+ and B sites are occupied by Mn^{3+} and Cu^{2+} with 96% and 4% occupancies, respectively, and all Mn ions are trivalent. The magnetic moments of Cu^{2+} on B sites were ignored. In contrast to $CuMnO_2$, a single group of magnetic Bragg reflections, which is assigned to $\boldsymbol{Q} = (\bar{\frac{1}{2}}\frac{1}{2}0)$, was observed, as can be clearly seen in the inset of Fig. 3(b). Considering the single component of $\boldsymbol{Q}$ observed in $Cu_{1.04}Mn_{0.96}O_2$, the secondary reflections assigned to $\boldsymbol{Q}_2$ in $CuMnO_2$ might be caused by a small amount of the impurity $Cu_{1+x}Mn_{1-x}O_2$ with $x \neq 0$. The difference in the c^* component of the $\boldsymbol{Q}$ vector corresponds to the stacking sequence in the c direction, which is antiferromagnetic in $\boldsymbol{Q}_1$ in $CuMnO_2$ and ferromagnetic in $Cu_{1.04}Mn_{0.96}O_2$. As shown in Fig. 3(b), we also fitted the experimental data of $Cu_{1.04}Mn_{0.96}O_2$. Table I lists the refined parameters. The direction and length of the magnetic moments are almost the same as those of $CuMnO_2$, although the stacking sequence in the c direction differs. The crystal structure is not monoclinic $C2/m$ but triclinic $C\bar{1}$ in $Cu_{1.04}Mn_{0.96}O_2$. The differences in α and γ from 90° [$\alpha = 90.12(1)$ and $\gamma = 89.87(1)$], which correspond to the degree of triclinic distortion in $Cu_{1.04}Mn_{0.96}O_2$, are somewhat smaller than those in $CuMnO_2$ [$\alpha = 90.18(1)$ and $\gamma = 89.84(1)$].

We here discuss the determined magnetic structures of $CuMnO_2$ and $Cu_{1.04}Mn_{0.96}O_2$. The schematic pictures of the magnetic structures are drawn in Fig. 4. In the ab plane, the stripe order occurs in both samples, which is drawn in Fig. 4(a).

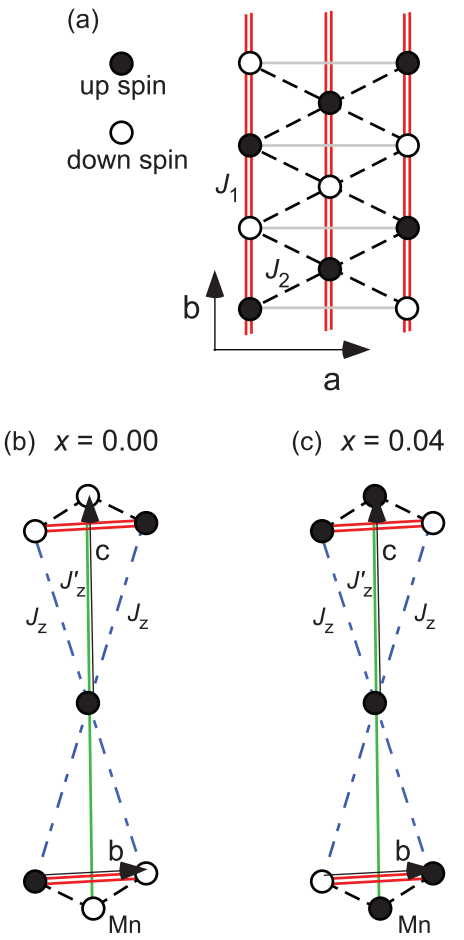

FIG. 4. (Color online) Schematic drawings of the magnetic structures in the (a) *ab* plane. (b) and (c) are illustrated to be differences in the stacking sequence between $CuMnO_2$ and $Cu_{1.04}Mn_{0.96}O_2$. Double solid, dotted, broken, and single solid lines denote the exchange interactions of J_1, J_2, J_z, and J'_z, respectively. Up and down spin parallel to the d_{z^2} orbital are illustrated by closed and open circles, respectively.

As was discussed in the previous paper,[10] the antiferromagnetic exchange interaction along the b axis, J_1, is larger than that along the apex direction in the isosceles triangles, J_2. In this case, the spin arrangement should be antiferromagnetic along the b axis. The triclinic lattice distortion, where $\alpha \neq 90^\circ$, lifts the doubly degenerate exchange energy along J_2, and leads to stripe ordering in both $CuMnO_2$ and $Cu_{1.04}Mn_{0.96}O_2$. On the other hand, the stacking sequences along the c axis are different from each other. The nearest-neighbor exchange paths bonding the interlayer spins are depicted by broken lines in Fig. 4(b), J_z. However, the exchange fields from the spins connected by J_z bonds are canceled out owing to the geometry. The next candidate to determine the stacking sequence is the second-nearest-neighbor interaction for interlayer interactions, which is illustrated by a single solid line as J'_z. As clearly seen in the comparison between Figs. 4(b) and 4(c), the difference in the stacking sequence between the two samples corresponds to the difference in spin arrangements along J'_z. It is naturally considered that the difference in the stacking sequence is caused by a change of sign of J'_z from antiferromagnetic

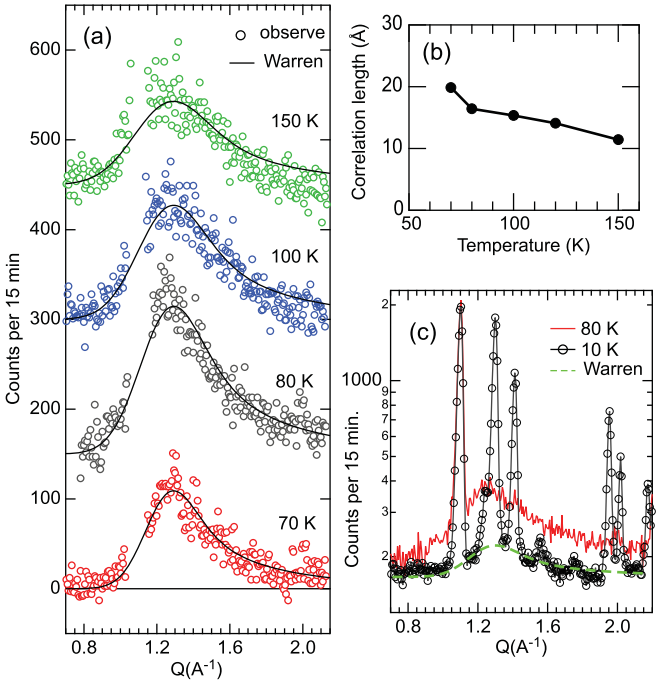

FIG. 5. (Color online) (a) Neutron diffraction patterns at four temperatures above $T_N = 64$ K in $CuMnO_2$. Circles show experimental data after removing the background data observed at 300 K, and the solid line is the fitted Warren line shape given by Eq. (1). (b) Temperature dependence of 2D correlation length. (c) Comparison of diffraction patterns obtained at 10 and 80 K. Dashed line denotes diffuse component (i.e., Warren component) at 10 K.

in $CuMnO_2$ to ferromagnetic in $Cu_{1.04}Mn_{0.96}O_2$. Since the d_{z^2} orbitals of Mn^{3+} are not aligned to the J'_z direction, the exchange path for J'_z is considered to be highly complicated. Therefore, when the atomic disorder induces Cu^{2+} and Mn^{4+} on the B sites in $Cu_{1.04}Mn_{0.96}O_2$, the exchange interaction along J'_z would be easily changed owing to the modification of the orbital state of Mn^{3+}.

Above T_N, we did not observe any magnetic Bragg reflections that correspond to 3D long-range ordering, rather we observed diffuse scattering in both $CuMnO_2$ and $Cu_{1.04}Mn_{0.96}O_2$, which indicates short-range ordering. As shown in Fig. 5, the magnetic diffuse scattering was asymmetric and has a maximum at $Q = 1.24$ Å^{-1}. The asymmetric peak shape is characteristic of 2D short-range order and it has the Warren line shape.[16] We subtracted the background at 300 K from the experimental data obtained at several temperatures and fitted the resulting data with the Warren function. It can be expressed as[16]

$$P(Q) = Cm \frac{F_{hk}^2 \left[1 - 2\left(\frac{\lambda Q}{4\pi}\right)^2 + 2\left(\frac{\lambda Q}{4\pi}\right)^4\right]}{\left(\frac{\lambda Q}{4\pi}\right)^{3/2}} \times \left(\frac{\xi}{\lambda\sqrt{\pi}}\right)^{1/2} F(a), \quad (1)$$

$$a = \frac{\xi\sqrt{\pi}}{2\pi}(Q - Q_0), \quad (2)$$

$$F(a) = \int_0^\infty \exp[-(x^2 - a)^2]dx, \quad (3)$$

where ξ is the 2D correlation length, C is a constant, m is the 2D multiplicity, and F is the 2D structure factor, which can be taken to be constant over small ranges of Q. As shown in Fig. 5(a), the experimental data are excellently fitted by the Warren function, indicating that the magnetic correlation above T_N can be characterized by 2D short-range ordering. Figure 5(b) shows the temperature dependence of the 2D correlation length, which was obtained by fitting with the Warren function. The correlation length increases from 11 Å at 150 K (which is about four times the in-plane lattice parameter, $4b$) to 20 Å ($\sim 7b$) at 70 K.

Figure 5(c) compares the diffraction patterns obtained at 80 and 10 K. Below T_N, the diffuse scattering component decreases, while the magnetic Bragg component increases rapidly. However, the diffuse scattering component is still detectable at 10 K, as the dashed line in Fig. 5(c) indicates. The remanent diffuse component has been reported in a previous study.[11] The result indicates that the 2D short-range order remains even at a temperature much lower than T_N. The remanent of the 2D correlation is discussed in the next section.

B. Magnetic excitations in $CuMnO_2$

1. *Inelastic neutron scattering*

Figures 6(a)–6(c) show excitation spectra in $CuMnO_2$. We observed the excitation spectrum with an energy gap of about 6 meV, as shown in Fig. 6(a). The spectral intensity decreases strongly with increasing Q, indicating magnetic excitation. Since 3D magnetic long-range ordering appears below T_N, we consider that the observed excitation originates from a spin wave excited from the magnetic ground state of $CuMnO_2$. The intensity increases above the energy gap of 6 meV and extends to about 18 meV, implying that the energy scale for magnetic exchange interactions is 12 meV (~140 K). This energy scale is the same order as the Curie-Weiss temperature ($\Theta_{CW} = -407$ K) obtained by susceptibility measurements.[10]

As shown in Figs. 6(b) and 6(c), quasielastic scattering is observed above T_N, which indicates strong thermal spin fluctuations. Figure 6(d) shows the temperature dependence of constant-Q scan profiles at $Q = 1.25$ Å^{-1}. Above T_N, we observed two components of incoherent elastic and quasielastic scattering; the former is described by a Gaussian profile with a width equivalent to the experimental resolution (1.6 meV) after resolution convolution and the latter has an asymmetric peak profile that depends on the temperature. The quasielastic component is expressed by the following dynamic structure factor:

$$S(\boldsymbol{Q},\omega) = C\frac{1}{1-\exp(-\hbar\omega/k_B T)}\cdot\chi(\boldsymbol{Q})\cdot\frac{\Gamma\omega}{\Gamma^2+\omega^2}, \quad (4)$$

where Γ is the broadening of the quasielastic component, $\chi(\boldsymbol{Q})$ is the static structure factor, and C is a constant. Since the width Γ is much higher than the experimental resolution, resolution correction was not performed in this study. As Fig. 6(d) shows, the experimental data at 150 and 80 K can be fitted by the dynamic structure factor described by Eq. (4), and Γ is refined to be 10.1 ± 1.1 and 5.9 ± 0.8 meV, respectively. Taking account of the above-mentioned elastic experiments that indicate 2D short-range ordering and the quasielastic scattering observed in the inelastic measurements, we consider that two-dimensionally correlated spins in space fluctuate dynamically above T_N.

With decreasing temperature, the intensity at $E = 4$ meV and $Q = 1.25$ Å^{-1}, which corresponds to the quasielastic scattering, increases down to 80 K and it then starts to decrease gradually below T_N [see inset of Fig. 6(d)]. This reduction in the quasielastic component corresponds to stabilization of the 3D magnetic long-range ordering, which is probed by the enhancement in the elastic intensity below T_N. However, the quasielastic component remains nonzero value relative to the background even at the lowest temperature 7 K [as indicated by the arrow in Fig. 6(d)]. We also observed the quasielastic signal in the constant-E scan at $E = 3$ meV, which has a maximum at $Q = 1.25$ Å^{-1} [Fig. 6(e)]. These results suggest that spin fluctuations exist except for the collective spin-wave excitation with an energy gap of 6 meV. The other peaks at $Q = 2.0$ Å^{-1} and $Q = 2.3$ Å^{-1} in Fig. 6(e) might be caused by acoustic phonons because several nuclear reflections (002, $\bar{2}01$, and 200) are observed in the Q region. As mentioned in the previous section, magnetic diffuse scattering was observed at the lowest temperature together with Bragg reflections [see Fig. 5(c)]. Diffuse scattering corresponding to 2D short-range ordering, which was observed in the elastic experiment, is considered to originate from spin fluctuations based on the inelastic measurements; this is discussed in the next section.

2. *Specific-heat measurements*

We first show the temperature dependence of ratio of the specific heat of $CuMnO_2$, $C(T)$, to the temperature. As shown in Fig. 7(a), a peak anomaly was observed at $T_N = 64$ K in $C(T)/T$. Since we did not observe any latent heat in the specific-heat measurements using relaxation methods, this phase transition is considered to be a second-order transition. No significant anomaly was observed at 45 K, where the weak ferromagnetic component appears in $CuMnO_2$.

We estimated the lattice specific-heat component, C_{latt}, assuming that C_{latt} obeys the Debye model, i.e., $C_{latt}(T) \propto T^3$ at low temperature. In the previous study, Debye temperature was estimated to be 600 K in $CuFeO_2$.[17] Using this value, we subtracted C_{latt} from observed $C(T)$ in the low-temperature region $T < 10$ K, and obtained the magnetic component C_{mag}. As shown in Fig. 7(b), C_{mag} is proportional to T^2 at low temperature, and the fitted line crosses the nonzero value at a temperature of 0 K. $C(T)$ is proportional to T^3 in conventional antiferromagnets with 3D order and no spin-wave energy gap. Based on the low-temperature C_{mag} data and the inelastic neutron-scattering data, we discuss the T^2 dependence of the C_{mag}. Since the energy gap for the collective spin-wave excitation is about 6 meV (~70 K) [see Fig. 6(a)], the low-temperature C_{mag} below $T^2 = 20$ K^2 ($T \sim 4.5$ K) has no contribution from spin-wave excitation with a large gap, but only from the remanent diffusive component.

Assuming that the spin correlation is two dimensional and using the linear spin-wave dispersion relation, $\omega = DK$, we can derive the T^2 dependence of $C(T)$.[18] ω is the spin-wave frequency, D is the spin stiffness constant, and K is the wave number. The internal energy is generally expressed as $U =$

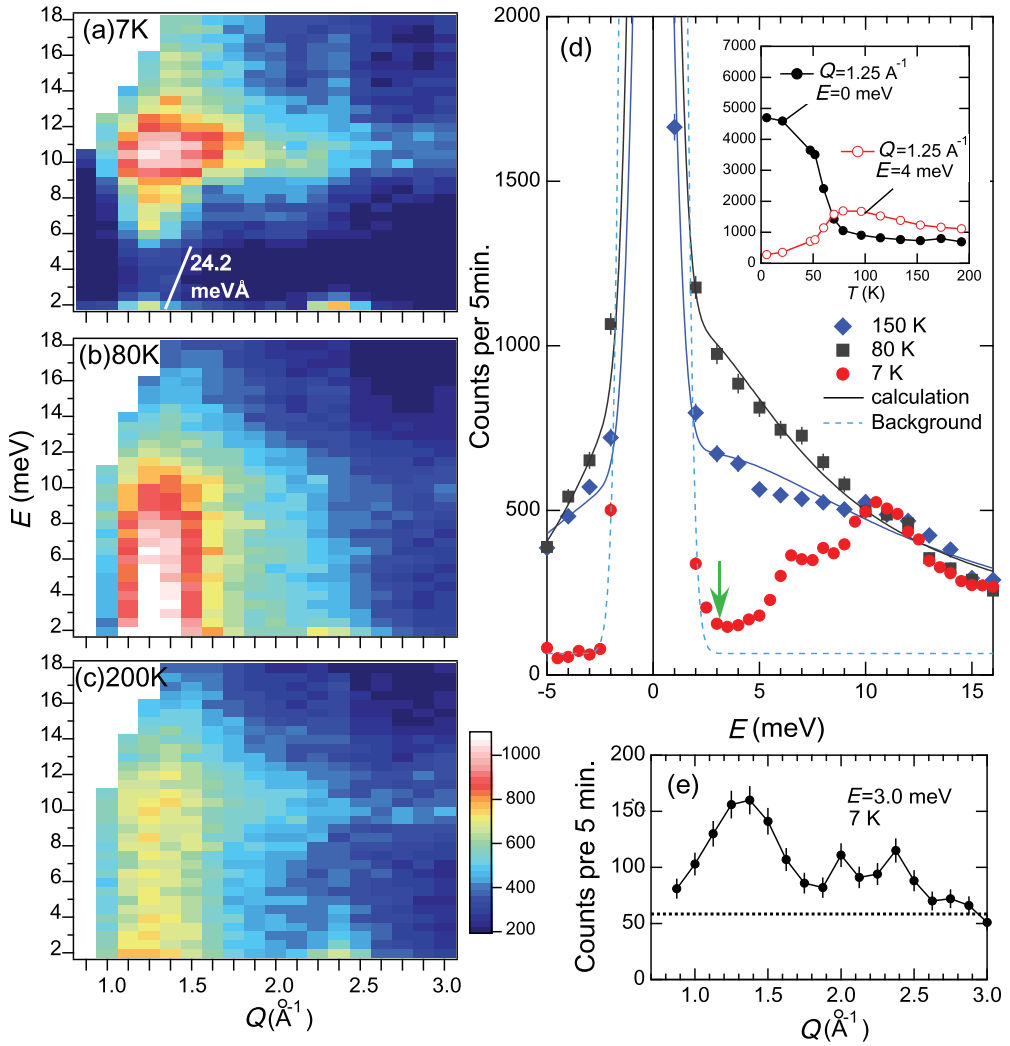

FIG. 6. (Color online) Excitation spectra represented as Q–E maps in $CuMnO_2$ at (a) 7, (b) 80, and (c) 200 K. For clarity, data for 7 K in (a) has been multiplied by a factor of 2. The spin-wave velocity of 24.2 meV Å, which is derived from the low-temperature specific-heat data, are drawn by a solid line in (a). (d) Temperature dependence of the constant-Q scan profiles at $Q = 1.25$ Å^{-1}. Symbols, solid lines, and dotted line, respectively, represent experimental data, the results of fitting the total intensity (described in the text), and the background. The inset shows the temperature dependence of the intensity for $E = 0$ meV and $Q = 1.25$ Å^{-1} and for $E = 4.0$ meV and $Q = 1.25$ Å^{-1}. (e) Constant-E scan profile for $E = 3.0$ meV at 7 K. The dotted line indicates the background.

$\int d\omega\, g(\omega) n(\omega) \hbar\omega$, where $g(\omega)$ is the density of states and $n(\omega)$ is the Bose-Einstein factor. The integration limits extend from a low-energy cutoff $\omega_0 = 2\pi D/L_0$ to the zone boundary. L_0 is the lower limit in the region over which the 2D linear dispersive mode propagates coherently. Therefore, for $\hbar\omega_0 \ll k_B T \ll k_B|\Theta_{CW}|$, the molar magnetic specific heat is expressed by

$$C_{mag}(T) = \frac{dU}{dT} = \frac{3ab\zeta(3)k_B^2 R}{\pi\hbar^2 D^2} T^2 - \frac{\pi abR}{L_0^2}, \qquad (5)$$

where

$$U = \lim_{\omega_D \to \infty} \frac{a^2 b^2 \hbar R}{4\pi D^2 k_B} \int_{\omega_0}^{\omega_D} d\omega \frac{\omega^2}{e^{\hbar\omega/k_B T} - 1}, \qquad (6)$$

where ω_D is the zone boundary frequency, $\zeta(3) = 1.202$, a and b are the lattice constants, and R is the gas constant. The spin stiffness constant D and L_0 were estimated by least-squares fitting the experimental data using Eq. (5) to be $\hbar D = 24.2$ meV Å and $L_0 = 417$ Å. As the solid line in Fig. 6(a) shows, the slope in the $S(\boldsymbol{Q},\omega)$ map, which is derived from the low-temperature specific-heat data, is reasonably consistent with the inelastic neutron-scattering results. The lower limit in the region over which the coherent mode propagates, L_0, is much larger than the two-spin correlation length, $\xi \simeq 20$ Å, obtained from the neutron diffraction experiments. As discussed in other studies for kagome $SrCr_{9p}Ga_{12-9p}O_{19}$ (Ref. 18) and triangular lattice $NiGa_2S_4$ (Ref. 19) systems, unlike observations of the two-spin correlation function in neutron diffraction measurements, specific heat probes excitations from all possible configurations. Consequently, we thus conclude that the remanent diffuse scattering component originates from spin liquid like 2D excitation, which is proved by $C_{mag}(T) \propto T^2$ in $CuMnO_2$.

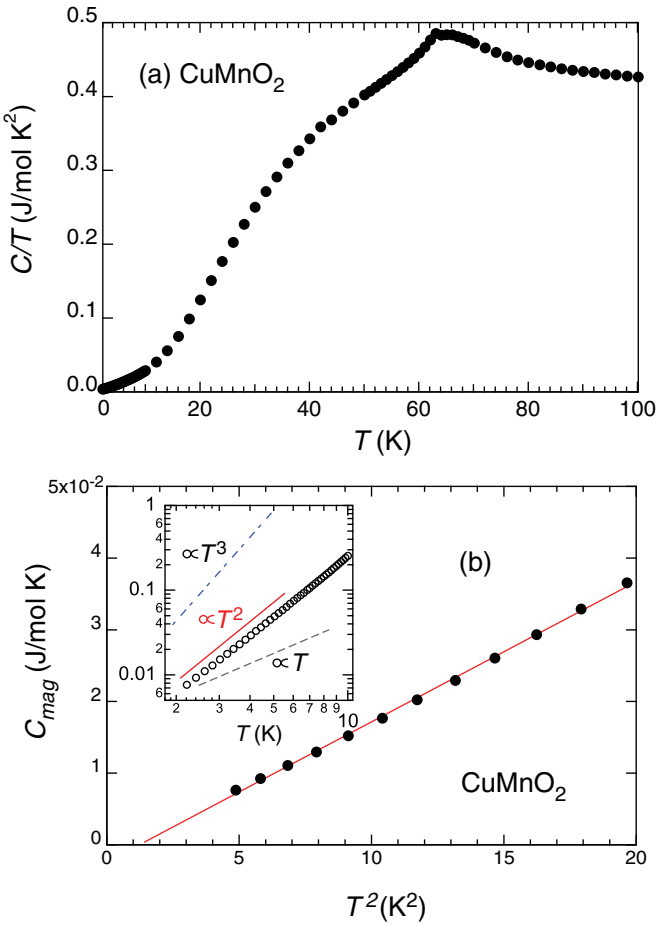

FIG. 7. (Color online) (a) Temperature dependence of the ratio of the specific heat, $C(T)$, of $CuMnO_2$ to T. (b) Low-temperature magnetic specific heat $C_{mag}(T)$ as a function of T^2. The solid line indicates the results of linear least-squaresfitting the data. The inset shows a plot of $C_{mag}(T)$ on a double logarithmic scale. The dotted, solid, and dashed lines are proportional to T, T^2, and T^3, respectively.

IV. SUMMARY

We have performed the magnetic susceptibility, specific-heat, elastic, and inelastic neutron-scattering experiments $Cu_{1+x}Mn_{1-x}O_2$ with $x = 0.00$ and 0.04. In $T_N < T < 300$ K, the temperature dependence of magnetic susceptibility in both samples shows the broad peak that is generally seen in the low-dimensional magnets.[13,14] In the neutron diffraction measurements on $CuMnO_2$, the diffuse scattering observed in $T_N < T < 300$ K is well fitted by Warren function,[16] proving the 2D short-range ordering. We also observed the quasielastic scattering in the inelastic neutron scattering in the temperature region in $CuMnO_2$. The magnetic correlations above T_N in both samples are characterized by 2D short-range order with strong spin fluctuations. Below T_N, the magnetic structures, with the propagation vectors $\boldsymbol{Q} = (\frac{\bar{1}}{2}\frac{1}{2}\frac{1}{2})$ in $x = 0.00$ and $\boldsymbol{Q} = (\frac{\bar{1}}{2}\frac{1}{2}0)$ in $x = 0.04$, have been identified to be collinear magnetic structures with the magnetic moments almost parallel to the d_{z^2} orbitals. Although the atomic disorder does not affect the direction and length of the magnetic moments in $CuMnO_2$, the stacking sequence along the c direction is changed from antiferromagnetic in $CuMnO_2$ to ferromagnetic in $Cu_{1.04}Mn_{0.96}O_2$. The second nearest-neighbor interlayer interaction, J_z', plays an important role for the magnetically stacking sequence owing to the canceled nearest-neighbor interlayer exchange fields. In the low-temperature region compared with T_N and the spin-wave gap, $C_{mag}(T)$ is proportional to T^2. Assuming two dimensionality and the linear dispersion relation, the $C_{mag}(T) \propto T^2$ can be explained, which is generally seen in spin-liquid-like systems.[18,19] We thus conclude that the magnetic excitation below T_N is characterized by not only collective spin-wave excitation with 6 meV energy gap from the 3D long-range magnetic order, but also spin-liquid-like 2D excitation in $CuMnO_2$.

Note added. Recently we became aware of the recent papers by Poienar *et al.*[20] and Garlea *et al.*[21] They also reported the magnetic ordering and the structural distortion in $Cu_{1+x}Mn_{1-x}O_2$ using their neutron diffraction data, which are consistent with the present results shown in Sec. III A 2.

ACKNOWLEDGMENTS

The authors wish to thank M. Kohno, N. Tsujii, and O. Yanagimachi for valuable discussions and helpful comments. This work was partly supported by Grants-in-Aid for Scientific Research "Young Scientists (B), Grant No. 20740209" from JSPS.

[1]Leon Balents, Nature (London) **464**, 199 (2010).
[2]P. Chandra and P. Coleman, Phys. Rev. Lett. **66**, 100 (1991).
[3]M. F. Collins and O. A. Petrenko, Can. J. Phys. **75**, 605 (1997).
[4]N. Terada, Y. Narumi, Y. Sawai, K. Katsumata, U. Staub, Y. Tanaka, A. Kikkawa, T. Fukui, K. Kindo, T. Yamamoto, R. Kanmuri, M. Hagiwara, H. Toyokawa, T. Ishikawa, and H. Kitamura, Phys. Rev. B **75**, 224411 (2007).
[5]T. Kimura, J. C. Lashley, and A. P. Ramirez, Phys. Rev. B **73**, 220401(R) (2006).
[6]S. Seki, Y. Onose, and Y. Tokura, Phys. Rev. Lett. **101**, 067204 (2008).
[7]K. Kimura, T. Otani, H. Nakamura, Y. Wakabayashi, and T. Kimura, J. Phys. Soc. Jpn. **78**, 113710 (2009).
[8]J. Topfer, M. Trari, P. Gravereau, J. P. Chaminade, and J. P. Doumerc, Z. Kristallogr. **210**, 184 (1995).
[9]M. Trari, J. Topfer, P. Dordor, J. C. Grenier, M. Pouchard, and J. P. Doumerc, J. Solid State Chem. **178**, 2751 (2005).
[10]J.-P. Doumerc, M. Trari, J. Topfer, L. Fournes, J.-C. Grenier, M. Pouchard, and P. Hagenmuller, Eur. J. Solid. State. Inorg. Chem. **31**, 705 (1994).

[11]F. Damay, M. Poienar, C. Martin, A. Maignan, J. Rodriguez-Carvajal, G. Andre, and J. P. Doumerc, Phys. Rev. B **80**, 094410 (2009).
[12]C. Vecchini, M. Poienar, F. Damay, O. Adamopoulos, A. Daoud-Aladine, A. Lappas, J. M. Perez-Mato, L. C. Chapon, and C. Martin, Phys. Rev. B **82**, 094404 (2010).
[13]T. Smith and S. A. Friedberg, Phys. Rev. **176**, 660 (1968).
[14]K. G. Srlvastava, Phys. Lett. **4**, 55 (1963).
[15]J. Rodriguez-Carvajal, Physica B **192**, 55 (1993).
[16]B. E. Warren, Phys. Rev. **59**, 693 (1941).
[17]O. A. Petrenko, G. Balakrishnan, M. R. Lees, D. M. Paul, and A. Hoser, Phys. Rev. B **62**, 8983 (2000).
[18]A. P. Ramirez, G. P. Espinosa, and A. S. Cooper, Phys. Rev. B **45**, 2505 (1992).
[19]S. Nakatsuji, Y. Nambu, H. Tonomura, O. Sakai, S. Jonas, C. Broholm, H. Tsunetsugu, Y. Qiu, and Y. Maeno, Science **309**, 1697 (2005).
[20]M. Poienar, C. Vecchini, G. André, A. Daoud-Aladine, I. Margiolaki, A. Maignan, A. Lappas, L. C. Chapon, M. Hervieu, F. Damay, and C. Martin, Chem. Mater. **23**, 85 (2011).
[21]V. O. Garlea, A. T. Savici, and R. Jin, Phys. Rev. B **83**, 172407 (2011).